

The Thousand-Pulsar-Array programme on MeerKAT VII: Polarisation properties of pulsars in the Magellanic Clouds

S. Johnston¹★, A. Parthasarathy², R. A. Main², J. P. Ridley³, B. S. Koribalski¹,
M. Bailes^{4,5}, S. J. Buchner⁶, M. Geyer⁶, A. Karastergiou^{7,8}, M. J. Keith⁹,
M. Kramer², M. Serylak^{10,11}, R. M. Shannon^{4,5}, R. Spiewak^{9,4,5},
V. Venkatraman Krishnan²

¹*Australia Telescope National Facility, CSIRO Space and Astronomy, PO Box 76, Epping NSW 1710, Australia*

²*Max-Planck-Institut für Radioastronomie, Auf dem Hügel 69, D-53121 Bonn, Germany*

³*School of Engineering, Murray State University, Murray, KY 42071, USA*

⁴*Centre for Astrophysics and Supercomputing, Swinburne University of Technology, Hawthorn, VIC 3122, Australia*

⁵*ARC Centre of Excellence for Gravitational Wave Discovery (OzGrav)*

⁶*South African Radio Astronomy Observatory (SARAO), 2 Fir Street, Black River Park, Observatory, Cape Town, 7925, South Africa*

⁷*Department of Astrophysics, University of Oxford, Denys Wilkinson Building, Keble Road, Oxford OX1 3RH, UK*

⁸*Department of Physics and Electronics, Rhodes University, PO Box 94, Grahamstown 6140, South Africa*

⁹*Jodrell Bank Centre for Astrophysics, Department of Physics and Astronomy, University of Manchester, Manchester M13 9PL, UK*

¹⁰*SKA Observatory, Jodrell Bank, Lower Withington, Macclesfield, SK11 9FT, United Kingdom*

¹¹*Department of Physics and Astronomy, University of the Western Cape, Bellville, Cape Town, 7535, South Africa*

Last updated; in original form

ABSTRACT

The Magellanic Clouds are the only external galaxies known to host radio pulsars. The dispersion and rotation measures of pulsars in the Clouds can aid in understanding their structure, and studies of the pulsars themselves can point to potential differences between them and their Galactic counterparts. We use the high sensitivity of the MeerKAT telescope to observe 17 pulsars in the Small and Large Magellanic Clouds in addition to five foreground (Galactic) pulsars. We provide polarization profiles for 18 of these pulsars, improved measurements of their dispersion and rotation measures, and derive the mean parallel magnetic field along the lines of sight. The results are broadly in agreement with expectations for the structure and strength of the magnetic field in the Large and Small Magellanic Clouds. The Magellanic Cloud pulsars have profiles which are narrower than expected from the period-width relationship and we show this is due to selection effects in pulsar surveys rather than any intrinsic difference between the population of Galactic and Magellanic objects.

Key words: pulsars:general, Magellanic Clouds

1 INTRODUCTION

More than 3000 radio pulsars have been discovered over the past 50 years, nearly all of which are located within our Galaxy and its associated globular cluster system. Only two external galaxies have had radio pulsars discovered within them; the Small and Large Magellanic Clouds (SMC and LMC hereafter). To date, seven radio pulsars have been discovered within the SMC and 22 within the LMC, all with the Parkes telescope (McCulloch et al. 1983; McConnell et al. 1991; Manchester et al. 1993; Kaspi et al. 1994; Crawford et al. 2001b; Manchester et al. 2006; Ridley et al. 2013; Titus et al. 2019). At distances of 62 kpc (SMC; Graczyk et al. 2020) and 50 kpc (LMC; Pietrzyński et al. 2019) these pulsars are

typically a factor of ten further than the pulsars detected in our Galaxy and hence their flux densities are very low.

In our own Galaxy, pulsars make excellent probes of the magneto-ionic interstellar medium (ISM). A pulsar’s dispersion measure (DM) is proportional to the integrated free-electron density along the line of sight and can be used to estimate the pulsar’s distance (e.g. Schnitzeler 2012; Yao et al. 2017). The rotation measure (RM), combined with the DM, allows the mean parallel magnetic field to be derived (e.g. Sobey et al. 2019), leading to models of the global magnetic field structure of the Galaxy (e.g. Noutsos et al. 2008; Han et al. 2018). Finally, the dynamic spectrum (e.g. Briskin et al. 2010) and long-term flux variability (e.g. Kumamoto et al. 2021) reveal the turbulence and inhomogeneous nature of the ISM. A similar approach has been attempted in the LMC and SMC in spite of the relatively small number of sight-lines available. Manch-

★ Email: simon.johnston@csiro.au

Table 1. Information for the observed pulsars. In the second column, SMC denotes pulsars in the Small Magellanic Cloud, LMC pulsars in the Large Magellanic Cloud and G pulsars in our Galaxy. The third column lists the observation time in minutes. Unless stated otherwise, values in columns 6 through 9 are from this work. Values in parentheses denote uncertainties in the last digit.

JNAME	ID	T_{obs} (min)	P (s)	$\log \dot{E}$ (erg s $^{-1}$)	DM (cm $^{-3}$ pc)	RM (rad m $^{-2}$)	S_{1400} (mJy)	$\Delta\nu_d$ (MHz)
J0045–7042	SMC	37	0.632336	32.5	71.3(3)	+31(3)	0.064(4)	
J0045–7319	SMC	10	0.926276	32.3	104.6(4)	–25(3)	0.25(1)	0.99(8)
J0111–7131	SMC	37	0.688542	32.9	79.4(5)		0.044(4)	1.0(3)
J0113–7220	SMC	10	0.325883	33.7	125.49(2)	+128(2)	0.189(8)	0.34(3)
J0131–7310	SMC	31	0.348124	33.2	205.22(6)	–57(3)	0.059(4)	
J0449–7031	LMC	30	0.479164	33.0	65.77(7)	+41(3)	0.056(4)	
J0455–6951	LMC	27	0.320423	34.0	94.70(2)	–26(1)	0.176(5)	0.30(2)
J0456–7031	LMC	14	0.800132	33.4	100.3(3) ^c		0.013(7)	
J0502–6617	LMC	5	0.691251	33.4	68.9(3) ^c			
J0519–6932	LMC	20	0.263212	33.1	118.86(2)	+85(6)	0.13(1)	0.21(5)
J0522–6847	LMC	37	0.674532	33.3	126.2(2)	–123(5)	0.083(3)	
J0529–6652	LMC	22	0.975737	32.8	103.31(7)	+9(2)	0.213(6)	0.12(3)
J0532–6639	LMC	36	0.642743	32.9	69.2(2)	+54(10)	0.042(4)	
J0534–6703	LMC	31	1.817565	33.4	95.3(1)	–35(1)	0.116(5)	0.24(6)
J0540–6919	LMC		0.050570	38.1	147.0(1) ^a	–246(1) ^a	0.10(3) ^a	0.00036 ^a
J0543–6851	LMC	42	0.708954	32.6	134.9(6)		0.087(4)	
J0555–7056	LMC	44	0.827838	32.6	72.9(1)	+26(6)	0.058(4)	1.6(2)
J0133–6957	G	5	0.463474	31.6	22.95(1)	20(5)	0.18(1)	4.6(4)
J0457–6337	G	43	2.497012	29.7	27.5(1.0) ^c	14(20) ^b	0.030(5)	
J0511–6508	G	24	0.322062	32.3	25.68(9)	27(6)	0.31(1)	4.8(6)
J0536–7543	G	21	1.245856	31.0	18.60(2)	26.1(1)	8.70(1)	3.0(3)
J0540–7125	G	27	1.286015	31.1	29.97(8)	40(2)	0.247(5)	2.2(2)

References: ^a Geyer et al. (2021), ^b Han et al. (2018), ^c Manchester et al. (2006).

ester et al. (2006) looked at the electron density distribution in the LMC, later updated by Yao et al. (2017). Use of extra-galactic RMs seen through the LMC (Mao et al. 2012) and SMC (Mao et al. 2008) allowed a model of their global magnetic fields to be constructed.

The radio luminosity of a pulsar at 1400 MHz, crudely defined as $L = S_{1400} d^2$ where S_{1400} is the flux density at 1400 MHz and d the distance in kpc, varies by several orders of magnitude across the population with only a mild dependence on its spin parameters (e.g. Szary et al. 2014). Although the distance determination in our Galaxy is subject to considerable uncertainty, the known pulsars in the Magellanic Clouds are at large distances and hence are amongst the most luminous pulsars known. Examination of the Magellanic pulsars can therefore indicate whether luminous pulsars are different from the less-luminous ones (Ridley et al. 2013) and/or whether distant pulsars have different characteristics to nearby ones.

In this paper we present observations from 22 pulsars, 17 of which are in the Magellanic Clouds. The observations and data analysis are described in Section 2 and Section 3 presents the polarization profiles and details on the individual pulsars. In Section 4 we discuss the implications of the results for the Magellanic Clouds and for the pulsar population.

2 SOURCE SELECTION, OBSERVATIONS AND ANALYSIS

For the purposes of pulsar observing, the MeerKAT telescope forms a tied-array beam on the sky from the coherent addition of its 64 individual antennas. The tied array beam has a full-width half-

maximum of some 6 arcsec at 1.4 GHz and hence the position of the pulsar needs to be known to an accuracy of a few arcsec. Of the 29 radio pulsars in the LMC/SMC, only 17 meet this criteria and are thus suitable for MeerKAT observations. In addition to these pulsars we observed a further 5 pulsars which are in the direction of the Magellanic Clouds, but located within our own Galaxy. Table 1 lists the observational details of the 22 pulsars observed. Column 2 denotes the location of the pulsars. Column 3 gives the total observing time, column 4 and 5 gives the pulsar spin period (P) and spin-down energy (\dot{E}) respectively.

Observations were conducted as part of the Thousand Pulsar Array (TPA) program, itself part of the larger MeerTime project. Details of the project as a whole and the observational setup can be found in Bailes et al. (2020) and Johnston et al. (2020). In brief, we used the observational band from 896 to 1671 MHz with 928 frequency channels. The data are folded into sub-integrations each of length 8 s for the duration of the observation and there are 1024 phase bins per pulse period. Polarization calibration is carried out using the procedures described in detail in Serylak et al. (2021). Data coming from the telescope have units of digitiser counts and we need to determine a multiplier to convert the units into mJy. To do this we assume that a single MeerKAT antenna has a system equivalent flux density of 390 Jy. We then use the number of antennas employed in conjunction with the bandwidth and observing time to compute the expected rms (in mJy) in a given frequency channel. The data are then scaled appropriately so that the actual rms matches the expected rms. Flux densities computed in this way are listed as S_{1400} in column 8 of Table 1. All these operations are carried out

by the processing pipeline `MEERPIPE`¹ which produces RFI-excised, polarisation- and flux-calibrated output products in `PSRFITS` format (Hotan et al. 2004). A more complete description of the pipeline is reported in Parthasarathy et al. (2021).

The dispersion measure (DM) is computed as follows. Using the pulsar ephemeris, we sum all the data in frequency and time to produce a noiseless, smoothed template. We also produce data summed in time and reduced to 32 frequency channels. The `PSRCHIVE` (Hotan et al. 2004) routine `PAT` is then used in conjunction with the template to produce a time-of-arrival of the profile in each of the frequency channels. These arrival times are then passed into `TEMPO2` (Hobbs et al. 2006) and a fit to the DM is made. The rotation measure (RM) is also computed from the same data set (i.e. time summed and with 32 frequency channels) via the routine `RMFIT`. The derived DMs, RMs and their uncertainties are given in columns 6 and 7 of Table 1.

We attempted to measure the scintillation bandwidth, $\Delta\nu_d$, for the pulsars at 1 GHz. For the foreground pulsars with $\Delta\nu_d$ greater than the channel bandwidth this was computed in the standard way via the auto-correlation function (ACF) of the dynamic spectrum (e.g. Johnston et al. 1998) over 50 MHz of bandwidth centered at 1 GHz. For pulsars with scintillation marginally unresolved at 1 GHz, $\Delta\nu_d$ was computed in 200 MHz centered on 1.4 GHz, and the value scaled to 1 GHz with a -4 index. For the remaining pulsars, $\Delta\nu_d$ was estimated via $m^2\Delta\nu$ where m is the modulation index and $\Delta\nu$ the channel bandwidth (e.g. Kerr et al. 2018). Measurements were made across the observing bandwidth and a power-law fit was obtained to yield the value at 1 GHz. Conservatively the uncertainty was set to 25% of the value (Kerr et al. 2018). Where obtainable, $\Delta\nu_d$ is listed in column 9 of Table 1. A more complete description of the methodology will be given in an upcoming paper on the scintillation properties of the entire TPA pulsar sample.

3 PULSAR PROFILES

The pulsar profiles are shown in Figures 1 through 3. Position angles are defined as increasing counter-clockwise on the sky (see Everett & Weisberg 2001) and are corrected to infinite frequency using the RM given in Table 1. Circular polarisation in pulsar astronomy uses the IEEE convention for left-hand and right-hand and so in the profiles shown here, left-hand circular polarisation is positive (van Straten et al. 2010). The linear polarization is corrected for bias following the prescription in Everett & Weisberg (2001). A brief description of the pulsars follows below.

3.1 LMC pulsars

The profiles of nine of the LMC pulsars are shown in Figure 1. Three pulsars are not shown. PSR J0502–6617 was not detected (albeit in a short 5 min observation) and PSR J0456–7031 has only a very low signal-to-noise ratio in a 14 min observation. PSR J0540–6919 is a young Crab-like pulsar which emits giant pulses (Johnston & Romani 2003; Geyer et al. 2021). The polarisation profile for this pulsar as seen by MeerKAT has been published separately by Geyer et al. (2021) and an RM of -246 rad m^{-2} was derived.

In general, the profiles of the nine pulsars are narrow, with only PSR J0543–6851 having a width greater than 20° . Three of the pulsars show clear evidence for a double-peaked structure, five

have a single component, and PSR J0522–6847 appears to have at least three components. The overall polarization fraction is low, typical also for the Galactic pulsars with similar spin-down energies (Johnston & Kerr 2018). The low polarization fraction coupled with the narrow profiles makes it hard to discern the swing of position angle and no conclusions can be drawn about the spin-axis orientation of these pulsars. Of the pulsars not observed, those presented in Ridley et al. (2013) are all single component profiles apart from PSR J0532–69 which is a narrow double. Polarization information for those pulsars is not available.

Our observations show that PSR J0529–6652 undergoes episodes of nulling, where the radio emission appears to cease. In the 22 min of observing, it is in the on-state for some 8 minutes and nulling for the remainder. The null states are several minutes in duration.

3.2 SMC pulsars

The profiles of the SMC pulsars are shown in Figure 2. Four of the five pulsars have profiles with narrow widths of less than 20° . Polarization fractions are generally weak, although PSR J0045–7042 has moderate linear polarization. We have derived RMs for four of the five pulsars. Two had previous measurements and our values are consistent with these but have much smaller uncertainties. We see evidence for wide-band diffractive scintillation at our observing frequency, with flux densities changing by a factor of a few between observations (see Section 4.3).

PSR J0045–7319 is a pulsar in a binary orbit with a B star companion (Kaspi et al. 1994; Bell et al. 1995). We have 12 observations of this pulsar made over a period of two years. Each observation is typically 6 mins in duration. In seven of these observations the pulsar is either not detected or extremely weak with a peak flux density below 2 mJy. In contrast, two observations have peak flux densities of 20 mJy. These variations are likely due to diffractive scintillation with a bandwidth comparable to the observing bandwidth. We also note that the pulsar has a steep spectral index and is much brighter at 660 MHz than at 1400 MHz. Previous polarization observations of the pulsar by Crawford et al. (2001a) taken at 660 MHz show a low level of linear polarization, relatively high circular polarization and a poorly constrained RM. Their low time-resolution indicates a simple Gaussian profile with a flat swing of PA. Our data at 1300 MHz show the profile has developed into a triple structure. The circular polarization is high, but the swing of position angle is very steep with indications of an orthogonal jump between the first two components.

3.3 Foreground pulsars

The profiles of four foreground pulsars are shown in Figure 3. Although PSR J0457–6337 was observed, its profile has a low signal-to-noise ratio and is not shown here. Its flux density of 0.02 mJy is considerably lower than quoted by Manchester et al. (2006) and likely the pulsar was in a low scintillation state in our observation. The profiles show a variety of morphologies, including one with three components (PSR J0540–7125), a trailing-edge dominant profile (PSR J0536–7543) and a wide single (PSR J0511–6508). For PSR J0511–6508 we have multiple, short observations. The flux density varies from 0.05 to 0.9 mJy due to the effects of diffractive scintillation and we quote the mean value in the table.

¹ <https://github.com/aparthas3112/meerpipe>

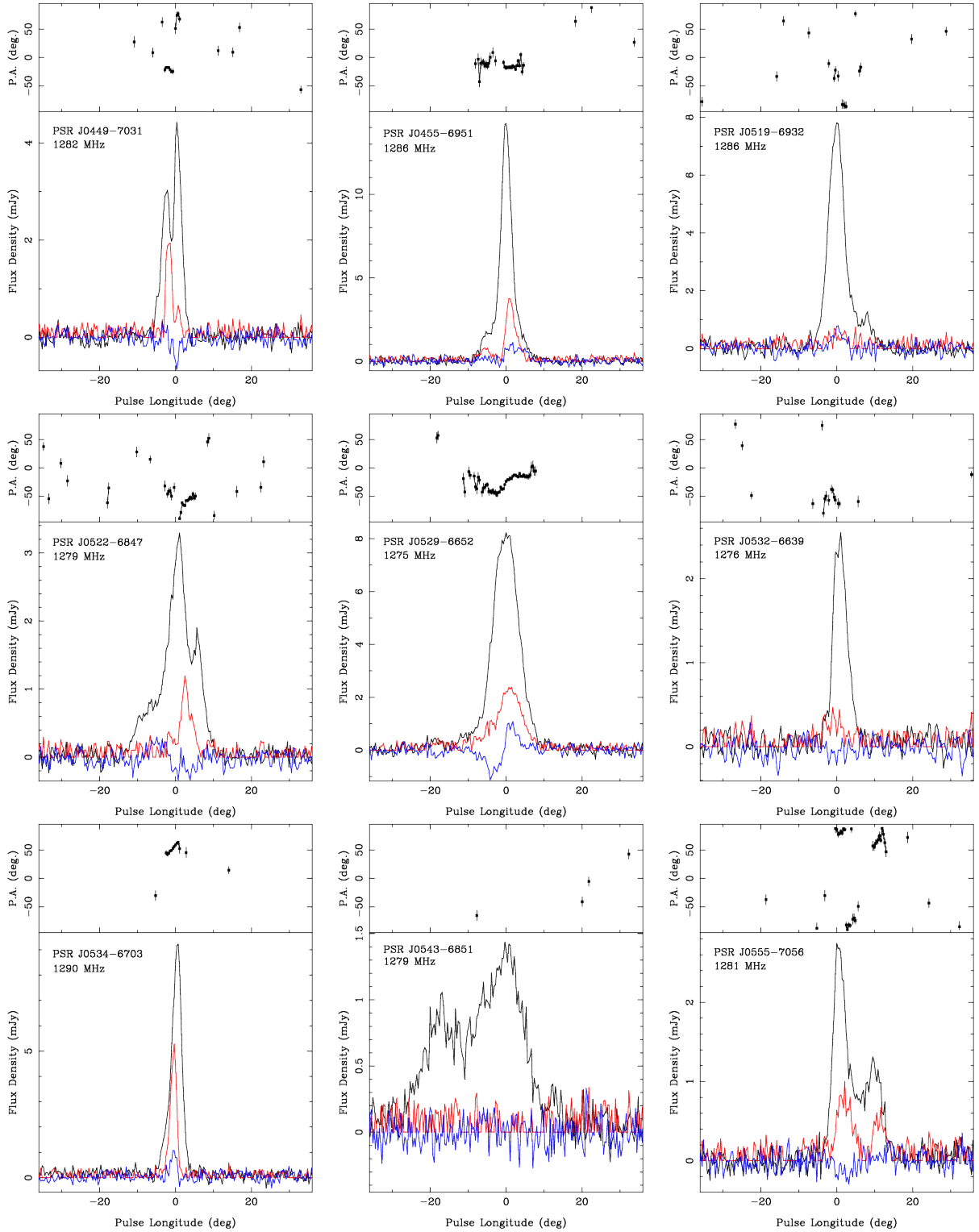


Figure 1. Polarisation profiles for the LMC pulsars. In the lower panels, the black line denotes Stokes I, the red trace shows the linear polarisation and the blue trace the circular polarisation. Left-hand circular polarisation is defined to be positive. The top panel shows the position angle of the linear polarisation, corrected to infinite frequency using the RM listed in Table 1. Position angles are only plotted when the linear polarisation exceeds 3 sigma. The zero point of pulse longitude is set to the peak of the total intensity profile.

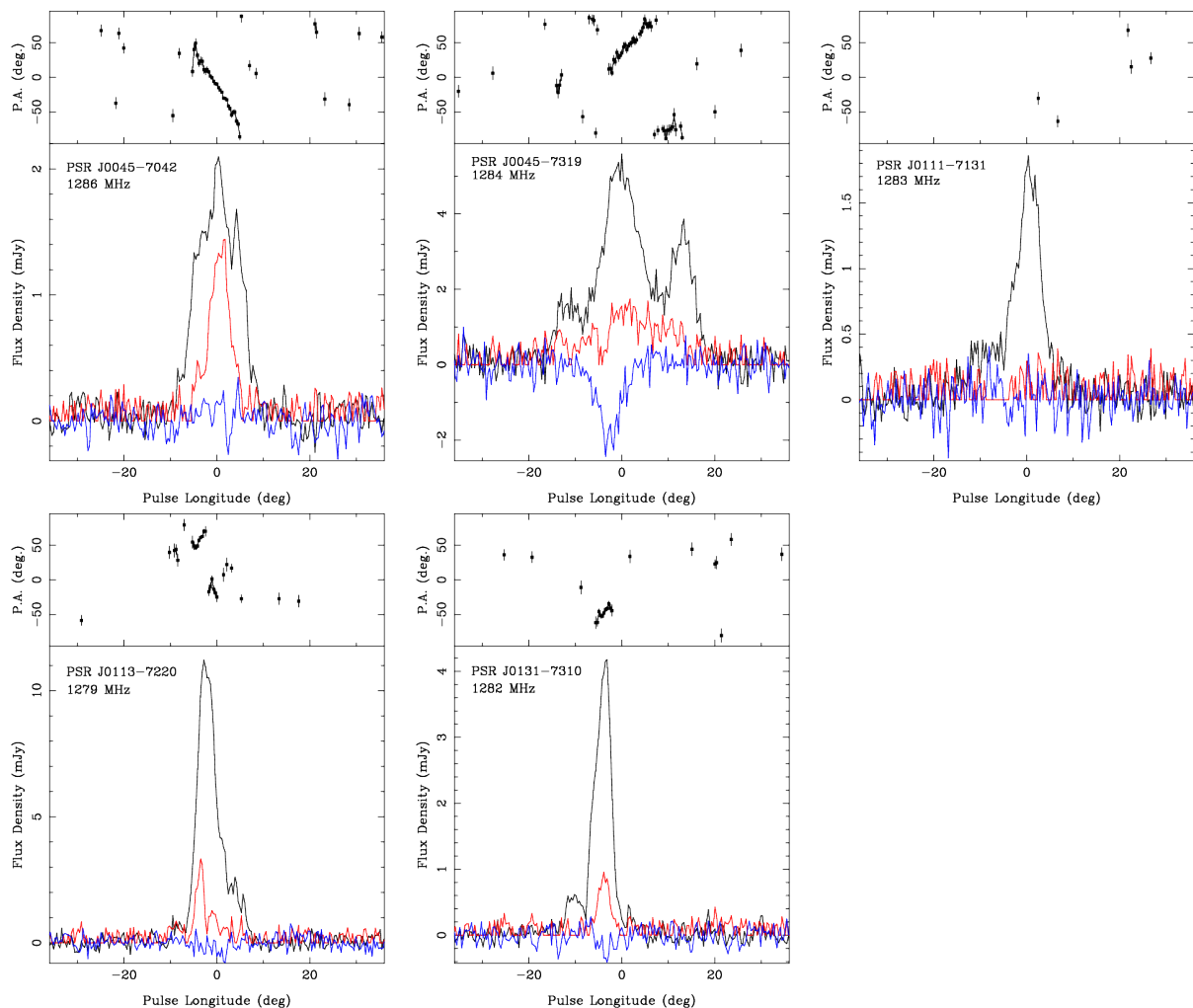


Figure 2. Polarisation profiles for the SMC pulsars. See Figure 1 for details.

4 DISCUSSION

4.1 The Magellanic Clouds

A comprehensive survey of the polarization properties and magnetic field structure of the LMC was carried out by Mao et al. (2012). The RMs of extragalactic sources seen through the LMC are potentially subject to several screens. The foreground, Milky Way, contribution to the RM is $+28 \text{ rad m}^{-2}$. The LMC has a diffuse halo which (on the near side of the disk) contributes -10 rad m^{-2} to the RM. Finally the body of the LMC appears to have an azimuthal magnetic field structure with a strength of $1 \mu\text{G}$ in addition to the presence of clumps, magnetic filaments, supernova remnants on smaller scales (Gaensler et al. 2005; Mao et al. 2012). To compute the RM contribution from the LMC, which we denote RM_c , we subtracted 28 rad m^{-2} from the observed RM values. Meanwhile, Yao et al. (2017) derived the contribution to the DM of the Galactic foreground material in the direction of the LMC pulsars. We use their Table 13 to compute DM_c , the DM contribution of the LMC to the overall pulsar DM. Table 2 lists DM_c and RM_c to the LMC pulsars given in Table 1. We also compute the inferred magnetic field parallel to the line of sight in μG via

$$B_{||} = 1.232 \frac{\text{RM}_c}{\text{DM}_c} \quad (1)$$

with DM_c and RM_c in conventional units. Table 2 shows a general trend that as the DM increases the RM becomes more negative. Four of the sight-lines have inferred $B_{||}$ significantly higher than the canonical $1 \mu\text{G}$.

In Figure 4 we show an image of the LMC taken from Kim et al. (1998). Superposed we show the pulsars (circles) from this work and the extragalactic sources (crosses) from Mao et al. (2012). The colours denote objects with net positive (green) and negative (light blue) values of RM (after subtracting the Galactic foreground contribution). The size of the symbols is proportional to the RM. As summarised by Mao et al. (2012), the RM values towards extragalactic sources behind the south-eastern part of the LMC are predominantly positive. PSR J0540-6919, the pulsar with the largest negative RM is located here. However, the very high negative RM and relatively high DM of this pulsar are almost certainly due to electron density content and the magnetic field of its parent plerion and supernova remnant (Brantseg et al. 2014). This is discussed further in Geyer et al. (2021). Five of our pulsars lie in regions where the extragalactic RMs are close to zero. These pulsars also possess RMs. Finally two of our pulsars, one with negative and one with positive RM, lie close to the centroid of the LMC where the extragalactic RMs also have mixed sign. In summary, with a limited number of sight-lines to pulsars it is difficult to draw conclusions,

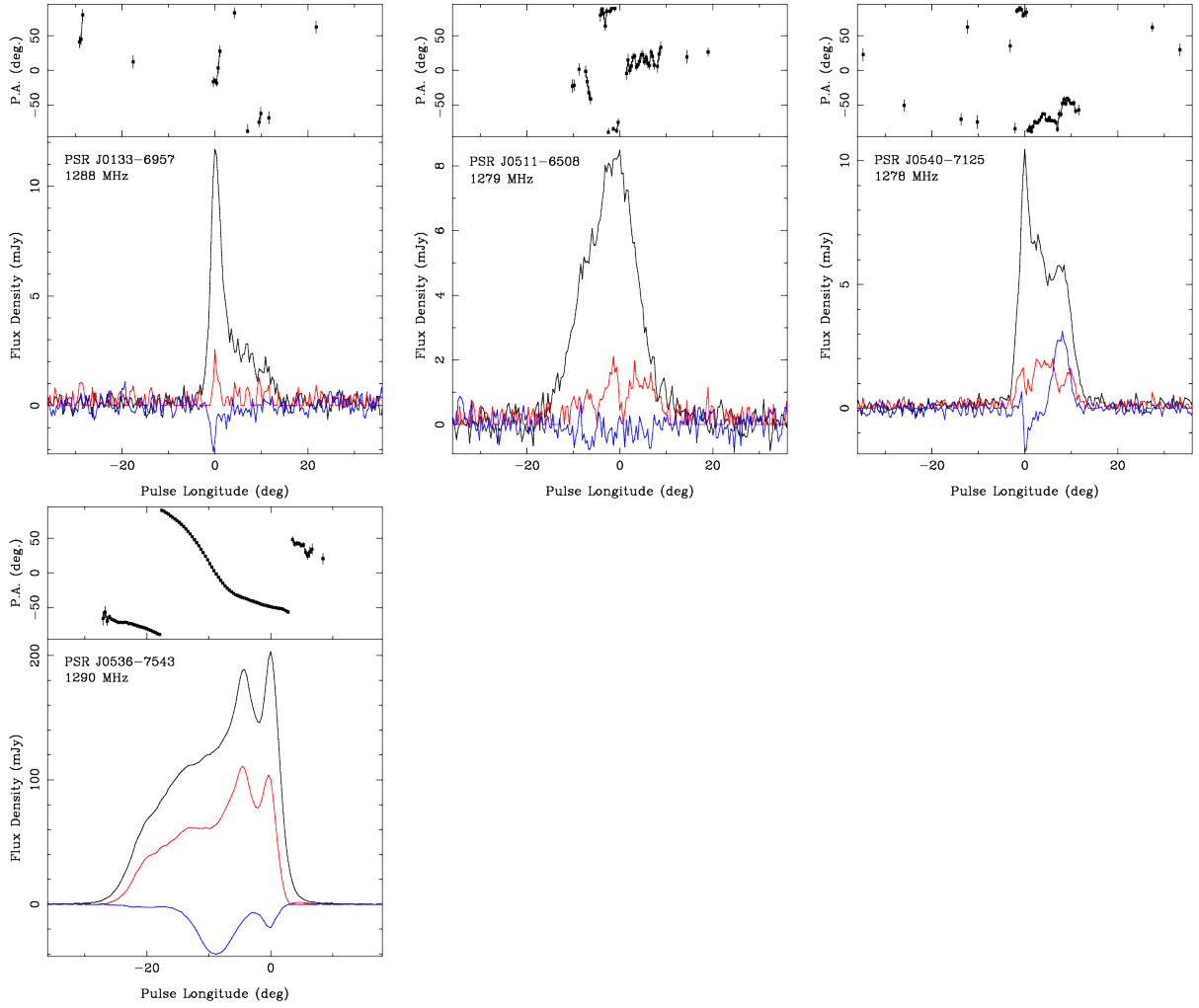


Figure 3. Polarisation profiles for the foreground pulsars. See Figure 1 for details.

Table 2. DM and RM contributions from the LMC to 12 pulsars, along with the derived value of $B_{||}$ from Equation 1.

JNAME	DM _c (cm ⁻³ pc)	RM _c (rad m ⁻²)	B (μG)
J0449-7031	16	+13	+1.0
J0455-6951	44	-54	-1.2
J0456-7031	51		
J0502-6617	19		
J0519-6932	62	+57	+1.1
J0522-6847	69	-151	-2.7
J0529-6652	45	-19	-0.5
J0532-6639	11	+24	+2.7
J0534-6703	35	-63	-2.2
J0540-6919	84	-274	-4.0
J0543-6851	71		
J0555-7056	6	-2	-0.4

but the results are broadly in line with the expectations of [Mao et al. \(2012\)](#) although it is clear from some high values of $B_{||}$ that structures local to the pulsar also contribute to the RM and DM.

Table 3. DM and RM contributions from the SMC to five pulsars, along with the derived value of $B_{||}$ from Equation 1.

JNAME	DM _c (cm ⁻³ pc)	RM _c (rad m ⁻²)	B (μG)
J0045-7042	41	1	0.1
J0045-7319	75	-55	-0.9
J0111-7131	50		
J0113-7220	95	+98	+1.3
J0131-7310	175	-87	-0.6

In the case of the SMC, [Mao et al. \(2008\)](#) estimate that the foreground Galactic material causes an RM of between 0 and ~ 50 rad m⁻². We have only one foreground pulsar with an RM of 20 rad m⁻². [Yao et al. \(2017\)](#) derive a DM of ~ 30 cm⁻³ pc for the Galactic foreground. In Table 3 we list DM_c and RM_c for the five SMC pulsars corrected for the foreground assuming a DM contribution of 30 pc cm⁻³ and an RM contribution of +30 rad m², along with the inferred magnetic field. [Mao et al. \(2008\)](#) examined ten extragalactic sources seen behind the SMC; nine of the ten had negative RMs with a median value of -75 rad m⁻². From Table 3, for

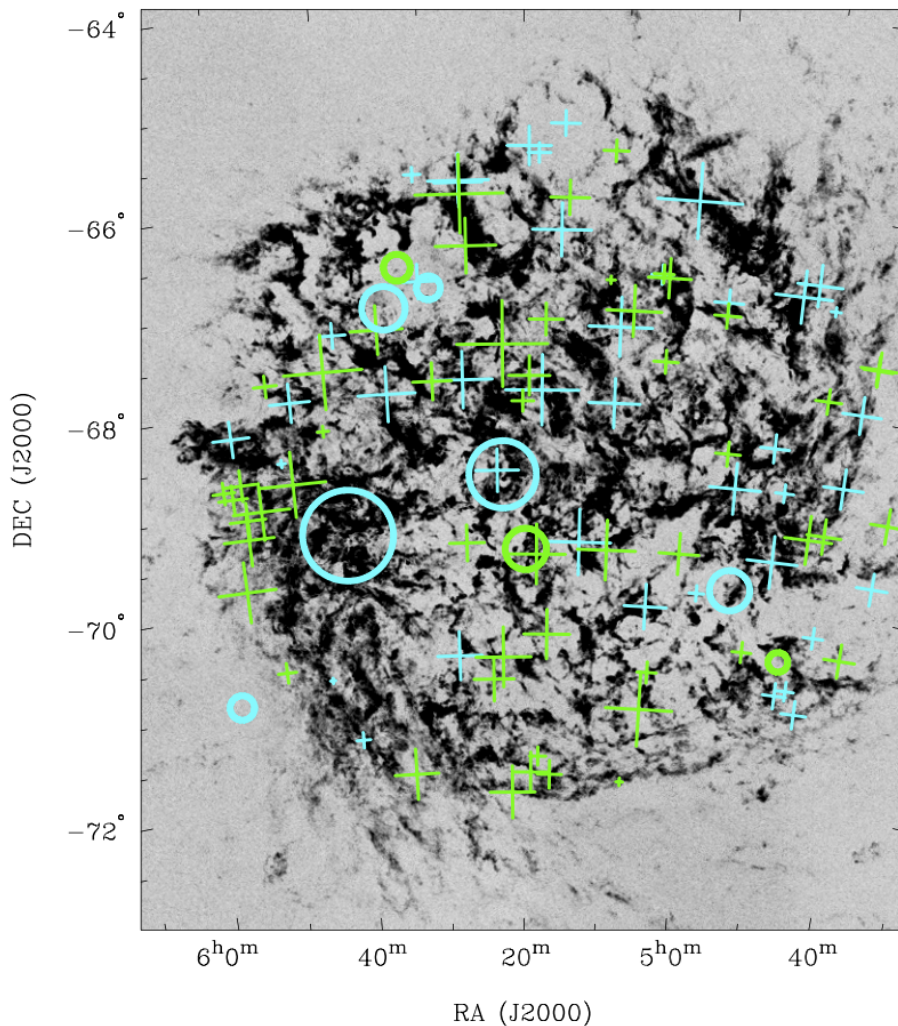


Figure 4. Greyscale image of the LMC, taken from [Kim et al. \(1998\)](#), with the intensity proportional to the peak flux density in the H I line. Crosses mark the location of the 93 extragalactic sources used by [Mao et al. \(2012\)](#). Circles mark the location of the nine pulsars with measured RMs. Green denotes sight-lines with positive RM, light blue sight-lines with negative RM. The area covered by the symbols is proportional to the RM.

the four pulsars two are negative, one consistent with zero and one (PSR J0113–7220) positive. Examination of the image of the SMC from [Dickel et al. \(2010\)](#) shows that PSR J0113–7220 lies outside the area containing the bulk of the radio continuum emission and there is no immediate explanation for its positive RM. The inferred magnetic fields are in-line with expectations for the SMC.

4.2 The pulsars

The SMC and LMC provide us with a set of 29 pulsars at distances beyond 50 kpc. The question arises as to whether there is any difference in the morphology of the profiles between these high-luminosity pulsars and pulsars at a distance of a few kpc. In the quasi-standard picture of pulsars, the radio emission arises at a low altitude above the polar-cap, the region bounded by the open field lines. In some models, emission arises from a central region (‘core’) and/or an annulus towards the outside of the beam (‘conal’) ([Rankin 1990](#); [Karastergiou & Johnston 2007](#)). Emission is seen only when the impact angle comes close to one of the magnetic poles. Core emission has a steep spectral index and dominates at low frequencies, whereas conal emission has a much flatter spectral index

and hence becomes dominant at higher frequencies. At 1.4 GHz where the majority of the MC pulsars have been found, a mixture of core and cones are seen. In this picture, the distance to the pulsar is not relevant and MC pulsars should have the same properties as Galactic pulsars. A contrasting model postulates emission in fan beams ([Wang et al. 2014](#); [Dyks & Rudak 2015](#)). The fan extends to much larger distances from the pulsar surface and hence emission at high impact angles is possible. As such high impact angles are rarely observed, [Wang et al. \(2014\)](#) surmised that the flux density would decrease as the impact angle increases. In this picture therefore, distant pulsars would be seen only at low impact angles unlike their nearby counterparts.

Disentangling differences in morphology between the profiles of MC pulsars and their Galactic counterparts is made more difficult by the severe selection effects in surveys for MC pulsars. Modern search techniques (whether Fourier transform or fast-folding based) are biased in favour of pulsars with narrow pulse profiles and against those with wider profiles ([van Heerden et al. 2017](#)). As we only detect 1 pulsar per 1000 in the LMC/SMC system ([Ridley & Lorimer 2010](#); [Titus et al. 2020](#)) then it comes as no surprise to see that the majority have narrow profiles. Furthermore, the lack of pulsars

Table 4. A comparison of measured widths (W_m) and expected widths (W_e) for four samples defined in the text. N denotes the total number in the sample.

Sample	N	$W_m < W_e$	$W_m = W_e$	$W_m > W_e$
LMC/SMC	23	48%	22%	30%
HTRU, $S < 0.25$ mJy	68	50%	24%	26%
HTRU, $S > 1.5$ mJy	169	36%	16%	49%
HTRU, $L > 125$ mJy kpc ²	49	28%	10%	61%

with $\dot{E} > 10^{34}$ erg s⁻¹ in the MCs (apart from PSR J0540–6919 which was not discovered in a blind survey), is likely because these pulsars tend to have wider profiles than their low \dot{E} counterparts (e.g. Johnston & Weisberg 2006).

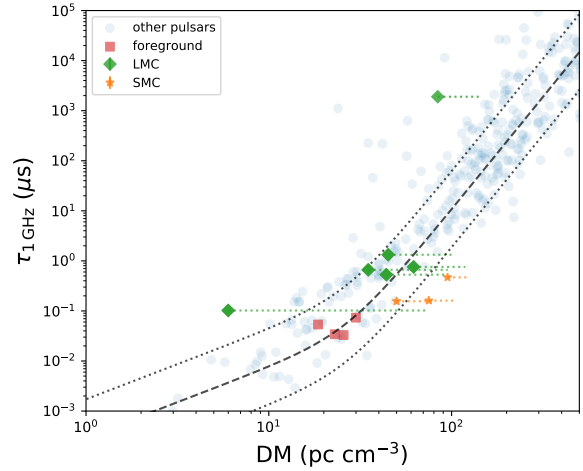
One potential approach is to compare the pulse widths of the MC pulsars with the Galactic counterparts also detected near the survey limit. If survey biases dominate, then we would expect that the pulsars would, on average, have smaller widths than expected. Conversely, we might expect the bright Galactic pulsars to have wider profiles on average. The MC pulsars typically have low flux densities (< 0.04 mJy) and are found near the survey detection limit. As a comparison set, we choose Galactic pulsars detected in the High Time Resolution (HTRU) survey with the Parkes telescope (Keith et al. 2010) with flux densities < 0.25 mJy. There are 225 such pulsars, of which only 11 (4.8%) have $\dot{E} > 10^{34}$ erg s⁻¹. This would imply that high \dot{E} pulsars are only marginally under-represented in the MC sample. For the bright pulsars we choose those with $S > 1.5$ mJy from the HTRU survey. There are 203 such pulsars of which 24% have $\dot{E} > 10^{34}$ erg s⁻¹.

Recently, Posselt et al. (2021) measured the profile width at 10% of the peak for many hundreds of pulsars and plotted these values versus the pulsar’s spin period, P . For any given P a large scatter in the pulse width is seen but Posselt et al. (2021) derived a best fit to the data and found that

$$W_e = 11.9 P^{-0.63} \quad (2)$$

where W_e is the expected width in degrees for P in seconds. They also measured values of the width, W_m , for 68 pulsars out of the 225 low flux density pulsars selected above and 169 of the bright sample. We can estimate values of W_m for 23 of the MC sample. We consider that $W_e = W_m$ if the difference is less than 2° , and otherwise crudely divide the sample into $W_e > W_m$ and $W_e < W_m$. Results are shown in Table 4. The LMC/SMC sample show a very similar width distribution to the low flux-density HTRU sample in that they favour narrow observed widths, whereas the bright pulsars from HTRU show evidence for wider pulsars than expectations. This clearly shows that the reason the MC pulsars have narrow profiles is due to the selection effects in pulsar surveys.

On the other hand, if distant (high luminosity) pulsars have low impact angle compared to nearby pulsars then their pulse width distributions should be different. Ridley et al. (2013) and Manchester et al. (2006) have shown that the luminosity function above 125 mJy kpc² is the same for Galactic and MC pulsars. In a similar fashion to above, we construct a high luminosity sample from the HTRU survey and take the pulse widths from Posselt et al. (2021). Results are shown in the bottom row of Table 4. We see that the profiles of the high luminosity Galactic sample are significantly wider than those of the Magellanic sample. This again demonstrates

**Figure 5.** Dispersion Measure versus scattering time for selected pulsars. Green diamonds and orange stars denote LMC and SMC pulsars respectively, red squares denote foreground pulsars and blue dots other pulsars with measurements from the literature. For each MC pulsar, the horizontal dotted lines connect the DM within the MCs to the total DM. The dash and dotted black lines show the fit of Cordes et al. (2016) and associated error estimation.

that the morphologies of the Magellanic pulsars are dominated by selection effects towards narrow profiles.

There remains a possibility that MC pulsars are inherently different to Galactic pulsars as, for example, the metallicity of the MCs is different to that in the Milky Way. This could manifest itself as a difference in initial spin and magnetic properties of the MC pulsars. With only a small number of pulsars at our disposal this is difficult to test, albeit attempted by Titus et al. (2020) for the SMC.

4.3 Scintillation

We were able to measure the diffractive scintillation bandwidth, $\Delta\nu_d$, for four of the foreground pulsars and eight of the brighter MC pulsars. For the low DM foreground pulsars, $\Delta\nu_d$ ranges from 2 to 5 MHz. For the MC pulsars, $\Delta\nu_d$ ranges from 0.1 to 1.6 MHz. In addition we include the measurement of scattering in PSR J0540–6919 by Geyer et al. (2021). There is a relationship between the scattering time (and therefore $\Delta\nu_d$) and DM for Galactic pulsars as given most recently by Krishnakumar et al. (2015) and Cordes et al. (2016). If we assume the scintillation in the MC pulsars is caused by the interstellar medium within the MCs themselves we can place these pulsars on the same relationship by using the DMs given in Tables 2 and 3.

Figure 5 shows scattering time versus DM for Galactic pulsars (from the literature) and the MC pulsars from this work in addition to the relationship of Cordes et al. (2016). The foreground pulsars fall nicely on the trend. For the LMC pulsars, PSR J0540–6919 has very large scattering for its DM. This scattering almost certainly arises from the pulsar’s parent supernova remnant in the same way as the Vela pulsar is heavily scattered by the Gum nebula. The other LMC pulsars fall on the trend, apart from PSR J0555–7056 for which it is possible that the DM contribution of the LMC has been underestimated by Yao et al. (2017). The three SMC pulsars appear slightly under-scattered, even though we expect the scattering to be a factor two higher than the standard Galactic case for a pulsar

with a screen located at half the pulsar’s distance. Again, the DM contribution from the Galaxy and its halo may be underestimated (and hence the SMC contribution overestimated) by Yao et al. (2017) and a discussion of this possibility can be found in Price et al. (2021). The flux density variations of more than a factor of 10 in PSR J0045–7319 could be from large-scale refractive effects, or the presence of an achromatic second screen near the pulsar. It is possible that the scintillation may still arise from the Milky Way rather than the MCs, which a single measurement of ν_d does not rule out. A measurement of annual variation in the scintillation timescale, or an angular broadening measurement would distinguish between the two cases.

5 SUMMARY

We have provided polarization profiles for 14 pulsars in the LMC and SMC and updates on their DMs and RMs. The inferred values of $B_{||}$ are in line with expectations for the LMC and SMC, although local conditions such as those around PSR J0540–6919 are also important. We show that the MC pulsars are narrower than expected from the period-width relationship of Posselt et al. (2021) and demonstrate that this is likely a selection effect in the pulsar surveys that detected them, rather than an intrinsic property of the pulsars themselves. The scintillation parameters for the pulsars in the LMC are broadly in line with expectations apart from PSR J0540–6919 which has enhanced scattering from its parent supernova remnant. In the SMC, the relatively low scattering may imply that the DM contribution from the Galactic halo is underestimated. Further observations are required to determine the location of the scattering screens.

Drawing significant conclusions from the data is hampered by the small number of known pulsars in the Magellanic system. In the near future, MeerKAT will survey the Magellanic Clouds for pulsars to a much greater depth than the previous Parkes surveys (Stappers & Kramer 2016). This should allow the ideas put forward in Sections 4.2 and 4.3 to be explored in more detail and should fill in the pulsar contribution to Figure 4. Finally, many more RMs to extra-galactic sources seen through the MCs should be made possible through the surveys on the ASKAP telescope (Johnston et al. 2008; Gaensler & POSSUM Collaboration 2010).

DATA AVAILABILITY

The data underlying this article will be shared on reasonable request to the corresponding author.

ACKNOWLEDGEMENTS

We thank G. Heald and D. Schnitzeler for useful discussions. The MeerKAT telescope is operated by the South African Radio Astronomy Observatory, which is a facility of the National Research Foundation, an agency of the Department of Science and Innovation. MeerTime data is housed and processed on the OzSTAR supercomputer at Swinburne University of Technology with the support of ADACS and the gravitational wave data centre via AAL. RMS acknowledges support through Australian Research Council Future Fellowship FT190100155. VVK acknowledges support from the Max-Planck Society.

REFERENCES

- Bailes M., et al., 2020, *PASA*, 37, e028
- Bell J. F., Bessell M. S., Stappers B. W., Bailes M., Kaspi V. M., 1995, *ApJ*, 447, L117
- Brantseg T., McEntaffer R. L., Bozzetto L. M., Filipovic M., Grieves N., 2014, *ApJ*, 780, 50
- Briskin W. F., Macquart J. P., Gao J. J., Rickett B. J., Coles W. A., Deller A. T., Tingay S. J., West C. J., 2010, *ApJ*, 708, 232
- Cordes J. M., Wharton R. S., Spitler L. G., Chatterjee S., Wasserman I., 2016, arXiv e-prints, p. arXiv:1605.05890
- Crawford F., Manchester R. N., Kaspi V. M., 2001a, *AJ*, 122, 2001
- Crawford F., Kaspi V. M., Manchester R. N., Lyne A. G., Camilo F., D’Amico N., 2001b, *ApJ*, 553, 367
- Dickel J. R., Gruendl R. A., McIntyre V. J., Amy S. W., 2010, *AJ*, 140, 1511
- Dyks J., Rudak B., 2015, *MNRAS*, 446, 2505
- Everett J. E., Weisberg J. M., 2001, *ApJ*, 553, 341
- Gaensler B. M., POSSUM Collaboration 2010, in *American Astronomical Society Meeting Abstracts #215*, p. 470.13
- Gaensler B. M., Haverkorn M., Staveley-Smith L., Dickey J. M., McClure-Griffiths N. M., Dickel J. R., Wolleben M., 2005, *Science*, 307, 1610
- Geyer M., et al., 2021, *MNRAS*, 505, 4468
- Graczyk D., et al., 2020, *ApJ*, 904, 13
- Han J. L., Manchester R. N., van Straten W., Demorest P., 2018, *ApJS*, 234, 11
- Hobbs G. B., Edwards R. T., Manchester R. N., 2006, *MNRAS*, 369, 655
- Hotan A. W., van Straten W., Manchester R. N., 2004, *PASA*, 21, 302
- Johnston S., Kerr M., 2018, *MNRAS*, 474, 4629
- Johnston S., Romani R. W., 2003, *ApJ*, 590, L95
- Johnston S., Weisberg J. M., 2006, *MNRAS*, 368, 1856
- Johnston S., Nicastro L., Koribalski B., 1998, *MNRAS*, 297, 108
- Johnston S., et al., 2008, *Experimental Astronomy*, 22, 151
- Johnston S., et al., 2020, *MNRAS*, 493, 3608
- Karastergiou A., Johnston S., 2007, *MNRAS*, 380, 1678
- Kaspi V. M., Johnston S., Bell J. F., Manchester R. N., Bailes M., Bessell M., Lyne A. G., D’Amico N., 1994, *ApJ*, 423, L43
- Keith M. J., et al., 2010, *MNRAS*, 409, 619
- Kerr M., Coles W. A., Ward C. A., Johnston S., Tuntsov A. V., Shannon R. M., 2018, *MNRAS*, 474, 4637
- Kim S., Staveley-Smith L., Dopita M. A., Freeman K. C., Sault R. J., Kesteven M. J., McConnell D., 1998, *ApJ*, 503, 674
- Krishnakumar M. A., Mitra D., Naidu A., Joshi B. C., Manoharan P. K., 2015, *ApJ*, 804, 23
- Kumamoto H., et al., 2021, *MNRAS*, 501, 4490
- Manchester R. N., Mar D. P., Lyne A. G., Kaspi V. M., Johnston S., 1993, *ApJ*, 403, L29
- Manchester R. N., Fan G., Lyne A. G., Kaspi V. M., Crawford F., 2006, *ApJ*, 649, 235
- Mao S. A., Gaensler B. M., Stanimirović S., Haverkorn M., McClure-Griffiths N. M., Staveley-Smith L., Dickey J. M., 2008, *ApJ*, 688, 1029
- Mao S. A., et al., 2012, *ApJ*, 759, 25
- McConnell D., McCulloch P. M., Hamilton P. A., Ables J. G., Hall P. J., Jacka C. E., Hunt A. J., 1991, *MNRAS*, 249, 654
- McCulloch P. M., Hamilton P. A., Ables J. G., Hunt A. J., 1983, *Nature*, 303, 307
- Noutsos A., Johnston S., Kramer M., Karastergiou A., 2008, *MNRAS*, 386, 1881
- Parthasarathy A., et al., 2021, *MNRAS*, 502, 407
- Pietrzyński G., et al., 2019, *Nature*, 567, 200
- Posselt B., et al., 2021, *MNRAS*. In Press.
- Price D. C., Flynn C., Deller A., 2021, *PASA*, 38, e038
- Rankin J. M., 1990, *ApJ*, 352, 247
- Ridley J. P., Lorimer D. R., 2010, *MNRAS*, 406, L80
- Ridley J. P., Crawford F., Lorimer D. R., Bailey S. R., Madden J. H., Anella R., Chennamangalam J., 2013, *MNRAS*, 433, 138
- Schnitzeler D. H. F. M., 2012, *MNRAS*, 427, 664
- Serylak M., et al., 2021, *MNRAS*, 505, 4483
- Sobey C., et al., 2019, *MNRAS*, 484, 3646

- Stappers B., Kramer M., 2016, in *MeerKAT Science: On the Pathway to the SKA*. p. 9
- Szary A., Zhang B., Melikidze G. I., Gil J., Xu R.-X., 2014, *ApJ*, 784, 59
- Titus N., et al., 2019, *MNRAS*, 487, 4332
- Titus N., Toonen S., McBride V. A., Stappers B. W., Buckley D. A. H., Levin L., 2020, *MNRAS*, 494, 500
- Wang H. G., et al., 2014, *ApJ*, 789, 73
- Yao J. M., Manchester R. N., Wang N., 2017, *ApJ*, 835, 29
- van Heerden E., Karastergiou A., Roberts S. J., 2017, *MNRAS*, 467, 1661
- van Straten W., Manchester R. N., Johnston S., Reynolds J. E., 2010, *PASA*, 27, 104

This paper has been typeset from a \LaTeX file prepared by the author.